Utah State University
DigitalCommons@USU

Space Dynamics Lab Publications | Space Dynamics Lab

1-1-2013

Noise Performance of the CrIS Instrument

Vladimir Zavyalov

Mark Esplin

Deron Scott

Benjamin Esplin

Gail Bingham

Erik Hoffman

See next page for additional authors

Follow this and additional works at: https://digitalcommons.usu.edu/sdl_pubs

Recommended Citation

Zavyalov, Vladimir; Esplin, Mark; Scott, Deron; Esplin, Benjamin; Bingham, Gail; Hoffman, Erik; Lietzke, Christopher; Predina, Joseph; Frain, Rebecca; Suwinski, Lawrence; Han, Yong; Major, Charles; Graham, Brandon; and Phillips, Lee, "Noise Performance of the CrIS Instrument" (2013). *Space Dynamics Lab Publications.* Paper 153.
https://digitalcommons.usu.edu/sdl_pubs/153

This Article is brought to you for free and open access by the Space Dynamics Lab at DigitalCommons@USU. It has been accepted for inclusion in Space Dynamics Lab Publications by an authorized administrator of DigitalCommons@USU. For more information, please contact digitalcommons@usu.edu.

UtahStateUniversity
MERRILL-CAZIER LIBRARY

Authors

Vladimir Zavyalov, Mark Esplin, Deron Scott, Benjamin Esplin, Gail Bingham, Erik Hoffman, Christopher Lietzke, Joseph Predina, Rebecca Frain, Lawrence Suwinski, Yong Han, Charles Major, Brandon Graham, and Lee Phillips

This article is available at DigitalCommons@USU: https://digitalcommons.usu.edu/sdl_pubs/153

Noise performance of the CrIS instrument

Vladimir Zavyalov,[1] Mark Esplin,[1] Deron Scott,[1] Benjamin Esplin,[1] Gail Bingham,[1] Erik Hoffman,[2] Christopher Lietzke,[2] Joseph Predina,[2] Rebecca Frain,[2] Lawrence Suwinski,[2] Yong Han,[3] Charles Major,[1] Brandon Graham,[1] and Lee Phillips[1]

Received 28 June 2013; revised 7 November 2013; accepted 19 November 2013; published 12 December 2013.

[1] The Cross-track Infrared Sounder (CrIS) is a spaceborne Fourier transform spectrometer (FTS) that was launched into orbit on 28 October 2011 onboard the Suomi National Polar-orbiting Partnership satellite. CrIS is a sophisticated sounding sensor that accurately measures upwelling infrared radiance at high spectral resolution. Data obtained from this sensor are used for atmospheric profiles retrieval and assimilation by numerical weather prediction models. Optimum vertical sounding resolution is achieved with high spectral resolution and multiple spectral channels; however, this can lead to increased noise. The CrIS instrument is designed to overcome this problem. Noise Equivalent Differential Radiance (NEdN) is one of the key parameters of the Sensor Data Record product. The CrIS on-orbit NEdN surpasses mission requirements with margin and has comparable or better performance when compared to heritage hyperspectral sensors currently on orbit. This paper describes CrIS noise performance through the characterization of the sensor's NEdN and compares it to calibration data obtained during ground test. In addition, since FTS sensors can be affected by vibration that leads to spectrally correlated noise on top of the random noise inherent to infrared detectors, this paper also characterizes the CrIS NEdN with respect to the correlated noise contribution to the total NEdN. Lastly, the noise estimated from the imaginary part of the complex FTS spectra is extremely useful to assess and monitor in-flight FTS sensor health. Preliminary results on the imaginary spectra noise analysis are also presented.

Citation: Zavyalov, V., et al. (2013), Noise performance of the CrIS instrument, *J. Geophys. Res. Atmos.*, *118*, 13,108–13,120, doi:10.1002/2013JD020457.

1. Introduction

[2] The first Joint Polar Satellite System (JPSS) suite of atmospheric instruments was launched into orbit on 28 October 2011 onboard the Suomi NPP (National Polar-orbiting Partnership, previously called National Polar-orbiting Operational Environmental Satellite System Preparatory Project) satellite. One of the instruments aboard JPSS is the Cross-track Infrared Sounder (CrIS), which is part of the Cross-track Infrared/Microwave Sounding Suite. CrIS is a sophisticated sounding sensor that accurately measures upwelling infrared radiance at very high spectral resolution [*Glumb and Jordan*, 2000; *Glumb et al*., 2002]. The CrIS observations data are delivered to the users in the form of the Raw Data Record, Sensor Data Record (SDR), and Environmental Data Record (EDR) [*Han et al*., 2013]. The science heritage for CrIS was derived from the Atmospheric Infrared Radiation Sounder (AIRS) on the NASA EOS Aqua satellite [*Aumann et al*., 2003] and Infrared Atmospheric Sounding Interferometer (IASI) on the European Metop platform [*Klaes et al*., 2007].

[3] In-flight performance and absolute accuracy of any sounding instrument is based on the basic design, ground-based calibration, and in-flight refinement of the calibration parameters. Instrument noise is a key performance parameter for mission success defining the lowest margin and quality of the measured radiances. Contemporary retrieval algorithms and numerical weather prediction (NWP) assimilation models use the radiance data from many spectral channels to retrieve atmospheric thermodynamic features with high vertical spatial resolution [*Smith et al*., 2009, 2012; *Barnet et al*., 2000]. High spectral resolution, many spectral channels, and low noise all serve to optimize the vertical resolving power of the sounding measurements. However, simply increasing the spectral resolution and number of channels in a sounding sensor degrade the signal-to-noise ratio (SNR) of each spectral channel. Therefore, reducing instrument noise is also important in realizing the benefits of a finer sounding sensor channelization to improve vertical resolution and absolute accuracy of soundings.

[4] Sensors that use a Fourier transform spectrometer (FTS) are usually affected by sampling errors, known as "Optical Path Difference (OPD) sampling jitters" which modify the desired positions of the interferometer moving

[1]Space Dynamics Laboratory, Logan, Utah, USA.
[2]ITT Exelis, Fort Wayne, Indiana, USA.
[3]NOAA Center for Satellite Applications and Research (STAR), Camp Springs, Maryland, USA.

Corresponding author: V. Zavyalov, Space Dynamics Laboratory, 1694 North Research Park Way, Logan, UT 84341, USA. (Vladimir.zavyalov@sdl.usu.edu)

©2013. American Geophysical Union. All Rights Reserved.
2169-897X/13/10.1002/2013JD020457

mirror along its scanning axis [*Zachor*, 1977]. These sampling errors may originate from mirror scanning speed variations in combination with stability of the optical components, electronic time delays, etc. An OPD sampling jitter leads to an interferogram signal distortion that increases total instrument noise, which in this case, is spectrally correlated over the whole spectral band. The increased spectral correlation of the noise could reduce information content and increase EDR retrieval and SDR assimilation errors if not properly accounted for [*Barnet et al*., 2000]. OPD sampling jitter caused by vibration susceptibility of the FTS instrument can lead to a very complicated and variable spectral correlation that can be difficult and sometimes impossible to take into account. In the JPSS CrIS program, special consideration and attention has been given to the instrument design and characterization of the total Noise Equivalent Differential Radiance (NEdN) to reduce and eliminate any possible sources of the spectrally correlated noise.

[5] This paper describes preflight and in-flight instrument noise performance with special attention to the spectrally correlated noise. The required accuracy of the instrument demands identifying and characterizing the noise including random and spectrally correlated error sources to lower the risk of poor instrument performance. For the JPSS project the CrIS instrument noise is characterized by the Noise Equivalent Differential Radiance (NEdN) which is an analog of Noise Equivalent Spectral Radiance [*Tobin et al*., 2006]. The operational SDR algorithm computes and reports NEdN for each field of view (FOV) using the 30 radiometrically calibrated internal calibration target (ICT) spectra within the 4 min moving window. NEdN is further averaged over 17 adjacent spectral bins to smooth the reported NEdN product for each FOV.

2. CrIS Instrument and Error Sources

[6] The CrIS instrument was designed, integrated, and tested by ITT Exelis. Overall infrared detection sensitivity is considerably better than similar types of hyperspectral instruments, particularly in the critical longwave infrared (LWIR) band, due to the large CrIS aperture and the use of photovoltaic (PV) detectors [*Glumb et al*., 2002]. Significant efforts during the instrument design and build phases were dedicated to the reduction and optimization of the total instrument radiometric errors and noise.

2.1. CrIS Instrument Overview

[7] CrIS is an FTS instrument with three spectral bands covering shortwave (SWIR), midwave (MWIR), and longwave (LWIR) infrared spectral bands from 2550 to 650 cm^{-1} (3.9 to 15.4 μm), each with a 3 × 3 array of circular sensing apertures at the focal plane forming nine field of views (FOV) of the instrument. The CrIS instrument has a number of design features that allow it to achieve high performance in a relatively small volume.

[8] The heart of the CrIS sensor is the interferometer, which was supplied by ABB Bomem. This module converts the incoming scene radiance into modulated interference patterns, which are then detected by the focal plane detectors. Extraneous modulations due to any jitter of the interferometer optical alignment must be minimized since this can produce signal distortion noise that degrades NEdN. The CrIS interferometer minimizes this noise source using dynamic optical alignment during the interferogram collection. A laser metrology is combined with multiple and spatially separated detections of the metrology wavefront error in two orthogonal axes of the interferometer to determine the moving mirror misalignment in real time. Alignment is actively restored using a servo feedback loop, which drives NEdN degradation caused by tilt to a negligible level. Additionally, a passive vibration-isolation system was integrated to enable CrIS to operate on the spacecraft with relatively high level of disturbances.

[9] A deep-cavity internal calibration target (ICT) and Deep Space (DS) view are used for radiometric calibration for improved accuracy. Spectral calibration is achieved using a combination of metrology laser at a wavelength of 1.55 μm and a reference neon lamp source for periodical calibration of the metrology laser. Spectral resolutions of the LWIR, MWIR, and SWIR spectral bands are 0.625 cm^{-1}, 1.25 cm^{-1}, and 2.5 cm^{-1}, respectively. CrIS has the capability to deliver 0.625 cm^{-1} spectral resolution in all three bands, and the NPP program will be archiving this full-resolution data.

[10] A critical CrIS design selection was the use of PV detectors in all three spectral bands. PV detectors have higher sensitivity and improved nonlinearity (NL) compared to photoconductive detectors. It was found that using the PV HgCdTe technology at all CrIS wavelengths was feasible but only if the detector temperature for the LWIR band could be kept below 85 K. Above this temperature, the PV detectors experience a large increase in noise level. Using passive cooling, CrIS was designed to meet this temperature requirement. The CrIS focal plane array assemblies were selected using module level measurements to minimize NL and noise [*Masterjohn et al*., 2003].

2.2. NEdN Modeling

[11] An important step in the design phase of the mission was to estimate and optimize the CrIS instrument noise performance. The required accuracy of the instrument demands identifying and characterizing the noise and error sources to lower the risk of poor instrument performance. ITT Exelis developed the CrIS NEdN model to predict system level performance based on relevant component data for each subassembly [*Schwantes et al*., 2002]. This includes geometrical and spectral characteristics of the optics, responsivity of the detectors, and electrical characteristics of the analog and digital electronics. Over the lifetime of the program, the model has been refined to incorporate the most influential noise contributions, with the goal of being able to approach theoretical performance limits.

[12] The on-orbit NEdN model predicts the total noise based on all the contributions listed below. These can be grouped into two categories, those directly involved with converting photons to a digital signal (1–7) and those that cause distortions of the interferogram (8–14). Many of the noises within the second category may also contribute to the correlated noise (9 and 11–14). As an aside, tilt-induced OPD sample jitter may also contribute to both the correlated and uncorrelated noise, though not at the vibration levels experienced on orbit. This effect, which was observed under high vibration conditions during preflight testing, results

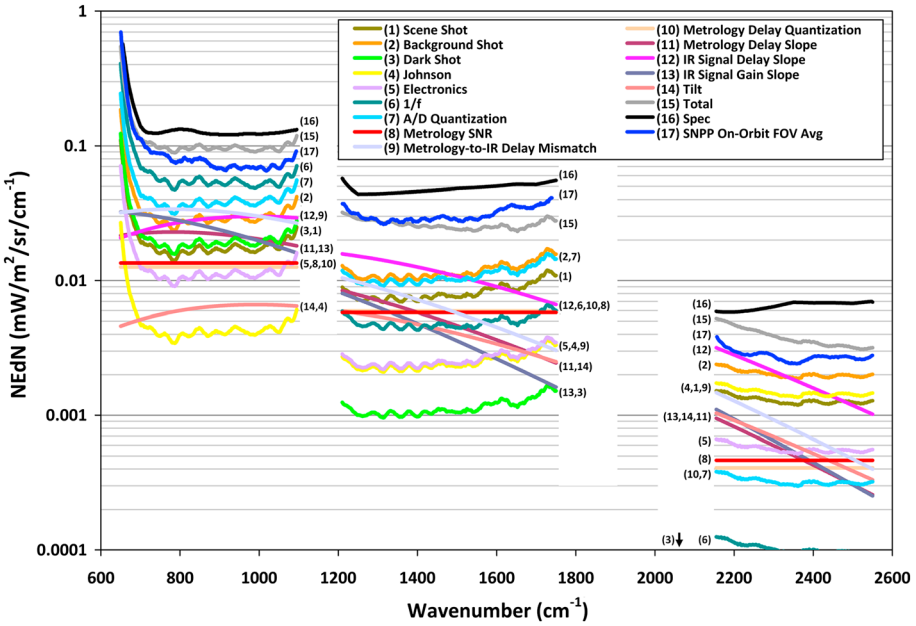

Figure 1. Comparison of modeled CrIS instrument noise (1–15) to both the spec (16) and the measured SNPP on-orbit performance (17).

from the error in the OPD sampling for off-axis detectors due to changes of OPD caused by mirror misalignment relative to center detector.

[13] 1. Scene shot—noise arising from the discrete nature of the scene radiance.

[14] 2. Background shot—noise arising from the discrete nature of the thermal emission from the optics.

[15] 3. Dark shot—noise arising from the discrete nature of the detector dark current.

[16] 4. Johnson—noise caused by thermal agitation in the detector and readout circuitry.

[17] 5. Electronics—noise attributable to electronic components between the detector's readout circuitry and the analog-to-digital (A/D) converter.

[18] 6. 1/*f*—noise with a 1/*f* frequency spectrum.

[19] 7. A/D quantization—noise caused by digitization in the A/D converter.

[20] 8. Metrology SNR—noise in the zero-crossings detection process can result in OPD sampling errors.

[21] 9. Metrology-to-IR delay mismatch—noise caused by post detection electronic delay mismatch of the metrology and IR signals when mirror velocity changes.

[22] 10. Metrology delay quantization—noise resulting from an additional quantization delay error on the metrology signal that occurs when tuning the metrology-to-IR delay match.

[23] 11. Metrology delay slope—delay variation of the metrology sampling signal after passing through a filter with nonflat delay versus frequency response due to speed variation of the moving mirror.

[24] 12. IR signal delay slope—distortion in the phase of the IR signal after passing through a filter with nonflat delay versus frequency response when the moving mirror speed changes.

[25] 13. IR signal gain slope—distortion in the amplitude of the IR signal after passing through a filter with nonflat frequency response when the moving mirror speed changes.

[26] 14. Tilt—any misalignment between the porch swing moving mirror and the dynamic alignment mirror will result in an unwanted modulation of the magnitude of the IR signal and contribute to the noise.

[27] The total modeled noise for CrIS on Suomi NPP (SNPP), along with all modeled noise contributions, is compared to specification and the SNPP on-orbit performance in Figure 1. As shown, the modeled LWIR and SWIR NEdNs are conservative, while the modeled MWIR NEdN is very close at longer wavelengths and tends to undershoot at shorter wavelengths. Observe that the most dominant noise contributions differ significantly across the bands. The 1/*f* noise is the most dominant in the LWIR band, less influential in the MWIR band, and negligible in the SWIR band. In the MWIR and SWIR bands, both background shot noise and noise due to the IR signal delay slope are the most dominant. Note that the spectrally correlated noise has negligible contribution to the preflight and in-flight instrument noise performance discussed later. Spectrally correlated noise was detected only under externally induced vibration. This means that the instrument noise model slightly overestimates interferometric noise, so background shot noise alone should actually be the most dominant contributor in both the MWIR and SWIR spectral bands.

3. Preflight CrIS Noise Performance

[28] The CrIS instrument was subjected to rigorous ground thermal vacuum (TVAC) testing to assess and optimize overall instrument performance under simulated nominal and extreme mission conditions. This test program was also designed to evaluate and extract initial radiometric, spectral, and geolocation calibration parameters/coefficients, which were then updated during in-flight calibration/validation (Cal/Val) activities [*Han et al.*, 2013; *Tobin et al.*, 2013]. Additionally, the CrIS sensor was subjected to the TVAC test after being integrated to the spacecraft.

[29] This section discusses the results of these ground tests, with an emphasis on the noise performance. Total instrument

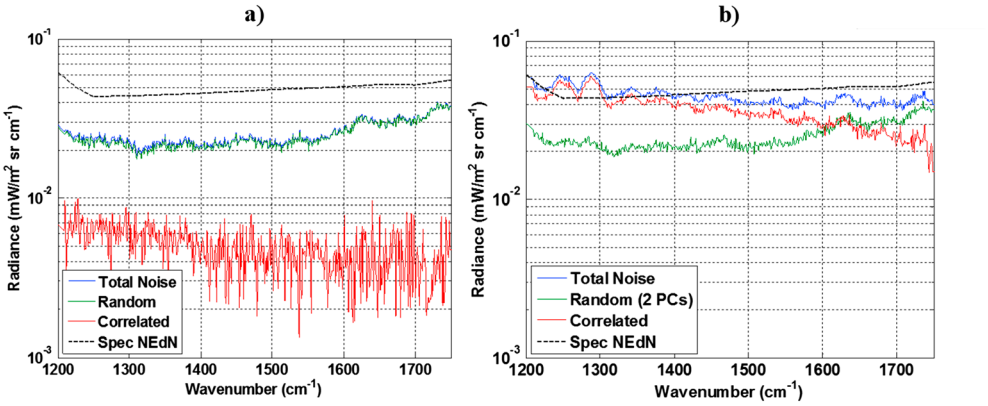

Figure 2. Correlated (red) and random noise (green) contribution to the total NEdN (blue) estimated from the ECT spectra acquired during dynamic interaction test for center FOV5 in MWIR spectral band. (a) Baseline NEdN is compared with (b) NEdN estimated for an external vibration of $5{\cdot}10^{-3}\,g_0$ injected along the Y axis at 158 Hz. Black line is a spec NEdN value.

noise (NEdN) is estimated as the standard deviation of the measured spectral radiance in a given wave number bin over a set of acquired blackbody samples and expressed in standard units of $\mathrm{mW/m^2/sr/cm^{-1}}$. During ground tests, three calibration blackbody targets were available for NEdN estimation, including ICT and DS calibration targets, and an External Calibration Target (ECT).

3.1. PCA Approach for Spectrally Correlated Noise Characterization

[30] Noise of a high-resolution spectral instrument can be either correlated or random (uncorrelated) in the spectral domain. The spectrally correlated noise can be found in FTS instruments when the vibration-induced errors caused by uncompensated Michelson mirror tilt and sampling jitter are present. The spectrally correlated noise component of the NEdN was estimated for the CrIS instrument using a principal component analysis (PCA) approach that was developed for the JPSS program. A detailed description of the PCA for noise estimation using a set of blackbody spectra is presented in *Zavyalov et al.* [2011].

[31] The total blackbody spectra noise variance can be represented as a sum of random and spectrally correlated noise components:

$$\mathrm{NEdN_t^2} = \mathrm{NEdN_r^2} + \mathrm{NEdN_c^2}. \tag{1}$$

[32] The total instrument noise, $\mathrm{NEdN_t}$, is estimated as the standard deviation of the measured spectral radiance in a given spectral channel over a set of acquired blackbody samples. A statistically representative set of ECT, ICT, or DS interferograms is collected and then radiometrically and spectrally calibrated using a standard SDR algorithm. The random noise component, $\mathrm{NEdN_r}$, is estimated by applying a standard PCA technique to the same data set. A minimum of $M \sim 150$ blackbody spectra is required for accurate NEdN analysis (typically $M = 150$-900). The PCA procedure of random noise estimation includes several steps outlined in *Antonelli et al.* [2004] and detailed in *Zavyalov et al.* [2011] specifically for the set of blackbody spectra. The main idea of this procedure is to filter out random noise from the reconstructed signal selecting an optimal number of principal components (PC). Random noise filtered out after reconstruction of the original data can be estimated as the standard deviation of the residual errors between the original (R^{obs}) and reconstructed data (R^{rec}):

$$\mathrm{NEdN_r}(\nu_i) = \sqrt{\frac{1}{M-1}\sum_{J=1}^{M}\left(R_{ij}^{\mathrm{rec}} - R_{ij}^{\mathrm{obs}}\right)^2}. \tag{2}$$

[33] Knowing the total noise and its random component, the correlated noise component, $\mathrm{NEdN_c}$, can be easily estimated according to equation (1). In our experience, only one PC needs to be retained to reconstruct typical blackbody spectra when random noise is dominant or comparable with spectrally correlated noise. More PCs (typically two to four) are needed for optimal reconstruction of the observed blackbody spectra when spectrally correlated noise dominates. Earth scene (ES) radiances are more complicated due to spectral correlation induced by the atmospheric constituents, and a larger number of PCs are retained to estimate the random noise component. Typically 30–60 PCs are needed for accurate noise estimation depending on the ES variability and number of instrument spectral channels.

[34] The main advantage of the PCA approach for random noise estimation is that it captures spectral correlation over the whole spectral band while the alternative approaches capture only the correlation within the specified spectral window as discussed in *Zavyalov et al.* [2011].

3.2. Dynamic Interaction Test

[35] A Dynamic Interaction test was performed in the vacuum during the prelaunch ground testing for the purpose of characterizing the impact of vibration on the CrIS noise performance. During this test, the CrIS vibration-isolation system was not installed and external vibrations were injected into the instrument frame in three directions. The vibration level was measured by several accelerometers installed onto the frame. An initial sweep over disturbance frequencies from 10 to 1000 Hz was performed to determine what frequencies CrIS was most sensitive. For the most sensitive frequencies of interest, several vibration acceleration levels were then tested peaking from $1{\cdot}10^{-3}$ to $25{\cdot}10^{-3}$ of the Earth's gravity (g_0).

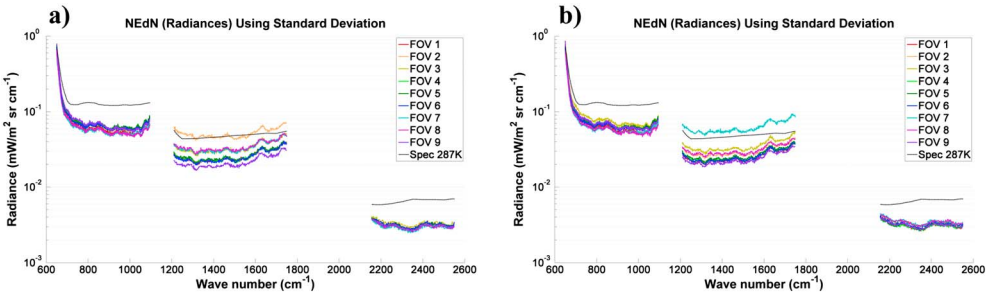

Figure 3. NEdN data measured during (a) TVAC3 and (b) TVAC4 tests at MN conditions at $T_{ECT} = 287$ K.

[36] The analysis of the dynamic interaction data allowed the CrIS team to understand instrument performance in the vibration environment and understand the signature of vibration-induced artifacts. Figure 2 is an example of the NEdN structure estimated for the center FOV of the CrIS MWIR spectral band. Figure 2a is the NEdN without vibration, while Figure 2b plots the random and correlated NEdN for the acceleration level of $5 \cdot 10^{-3}\, g_0$ applied to the frame. The increase in total noise during the vibration test for all vibration frequencies tested was mostly due to the spectrally correlated component. The highest instrument vibration sensitivity was observed at the frequencies near an interferometer mechanical resonance of 158 Hz. At other instrument sensitive frequencies (120, 149, 185, 240, and 617 Hz), the total estimated noise was also slightly elevated by 10–15% but still remained lower than the mission requirement level. As expected, the external vibration had the largest effect on the corner FOVs, a smaller effect on side FOVs, and the smallest on the central FOV5 which is consistent with the FOV off-axis angle. In the spectral domain, the SWIR band exhibited higher sensitivity to the external vibration as compared to other spectral bands. This observation confirms the results of NEdN modeling showing larger contribution of interferometric noise in the SWIR spectral band (see section 2.2).

3.3. TVAC NEdN Analysis

[37] For the JPSS program, TVAC tests were performed in several stages (TVAC1–TVAC4) testing different parameters of the CrIS instrument and its systems. This paper primarily focuses on reporting on the CrIS testing results in final TVAC3 and TVAC4 tests under the Mission Nominal (MN) conditions. In addition to MN, the CrIS instrument has been conservatively tested at Proto-Qual mission High (PQH), and Proto-Qual mission Low temperatures. The MN conditions best represent the on-orbit environment, and the results presented here represent expected on-orbit system performance.

[38] Figure 3 shows the NEdN results from TVAC3 (Figure 3a) and TVAC4 (Figure 3b), which were performed under MN thermal conditions. Radiometric and noise performance were measured with a high-performance blackbody target (ECT) adjustable in temperature range from 230 K to 330 K. As shown in Figure 3, the noise performance of the CrIS instrument during the TVAC tests was excellent and met mission requirements with an approximate 100% margin in all three bands (except for one MWIR FOV7 detector discussed later). PCA analysis showed that the total NEdN was dominated by the random noise component, as illustrated in Figure 4 for MWIR (Figures 4a and 4b) and SWIR FOV 7 (Figure 4c). The level and structure of the noise is consistent with the intrinsic detector noise discussed in section 2.2.

[39] Several minor NEdN outages were observed during different steps of TVAC testing. Most of these outages were observed during PQH conditions when instrument temperature was maintained at 310 K, which significantly exceeded the nominal on-orbit operating temperature of ~280 K. Outages of ~5% in LWIR occurred in several spectral channels along the far longwave "tail" and near the 700 cm^{-1} part of the spectrum. PCA analysis showed that LWIR outages were mostly due to the random component of the NEdN characteristic for the intrinsic $1/f$ detector noise (see Figure 1). These outages, occurring at the higher than normal operating temperatures, were directly related to the optical transmission of the ZnSe beamsplitter when background radiance emitted by the instrument itself was highest.

[40] Small outages in MWIR and SWIR spectral band were observed for several corner FOVs during TVAC4 test. This additional noise was due to the correlated noise component. An example of out of spec NEdN in SWIR during PQH test is shown in Figure 4d and compared with nominal observations during MN TVAC3 (Figure 4c). As was evident from the dynamic interaction testing, the SWIR spectral band is most sensitive to the vibration-induced sampling jitter. The root cause of these outages was identified as a tilt-induced OPD sample jitter due to vibration originating from test facility cryocooler and vacuum pumps.

[41] The TVAC testing also showed that several of the MWIR detectors, including FOV7, exhibited higher noise after they were thermal cycled from cryogenic to ambient temperature through the test program. The change in the MWIR NEdN level during consecutive TVAC tests occurred in FOVs 2, 3, 7, and 8. This change in NEdN can be seen in Figure 3 between TVAC3 and TVAC4 for MWIR FOV 2 and FOV7. These results show that FOV2 was out of spec during TVAC3 but within spec during TVAC4, while the NEdN of FOV7 has increased during TVAC4. In both cases, a random noise component dominated the total NEdN, as shown in Figures 4a and 4b.

[42] Continuous degradation of the MWIR NEdN (including FOV7) was not observed during all TVAC tests: once the detector cool-down process was completed, the detector noise stabilized. The root cause of this behavior was isolated to the HgCdTe detector material that changes parameters with warm-up/cool-down cycles. Migrating impurities in the IR diode interfaces can create/change trap states during

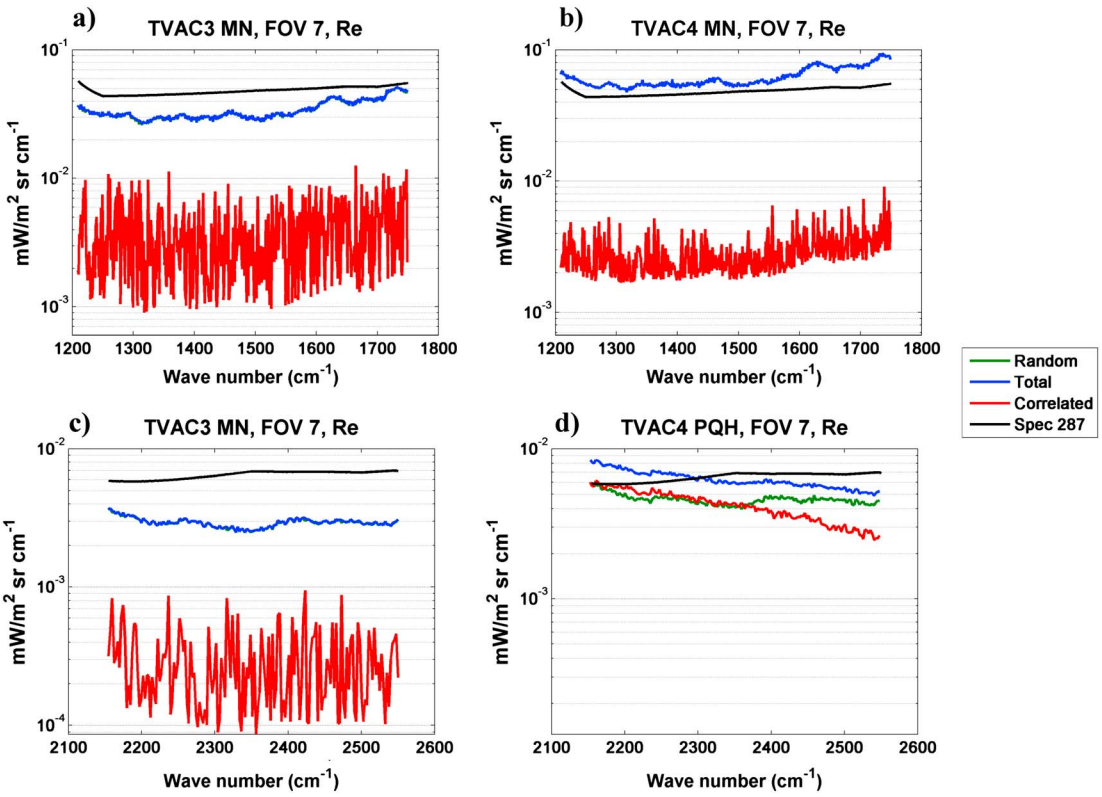

Figure 4. Random and correlated noise contributions to the total NEdN measured during (a, c) TVAC3 and (b, d) TVAC4 MN and PQH tests at $T_{ECT} = 287$ K for MWIR FOV7 (in Figures 4a and 4b) and SWIR FOV7 (in Figures 4c and 4d). Note that the blue line (total noise) overlays the green line (random noise) in Figures 4a, 4b, and 4c.

warm-up/cool-down cycles. Analysis of spacecraft TVAC test results has shown that the CrIS instrument noise has since remained stable and comparable to the last instrument level TVAC4 test shown in Figure 3b.

4. In-Flight NEdN Performance

[43] During TVAC testing, the CrIS SDR team used a 287 K external calibration (ECT) target to characterize instrument noise performance. On orbit, the CrIS ICT and DS views are used to characterize noise performance. Earth scene (ES) radiances contain information mostly on the atmospheric induced spectral correlation; therefore, it is practically impossible to extract information about the correlated noise induced by the instrument when viewing Earth scenes. Thus, for total and random NEdN estimation ICT and DS spectra are used, while random NEdN component is also estimated analyzing a set of ES data (2000–3000 spectra) through the PCA tools. ICT radiances are corrected for temperature drift using ICT temperature reading. The noise in the imaginary part of the SDR spectra when viewing each of the three targets is extremely sensitive to the various instrument mechanisms that can produce noise. Thus, a very useful diagnostic tool exists when using the same PCA technique outlined above when applied to the imaginary ICT, DS, and ES spectra.

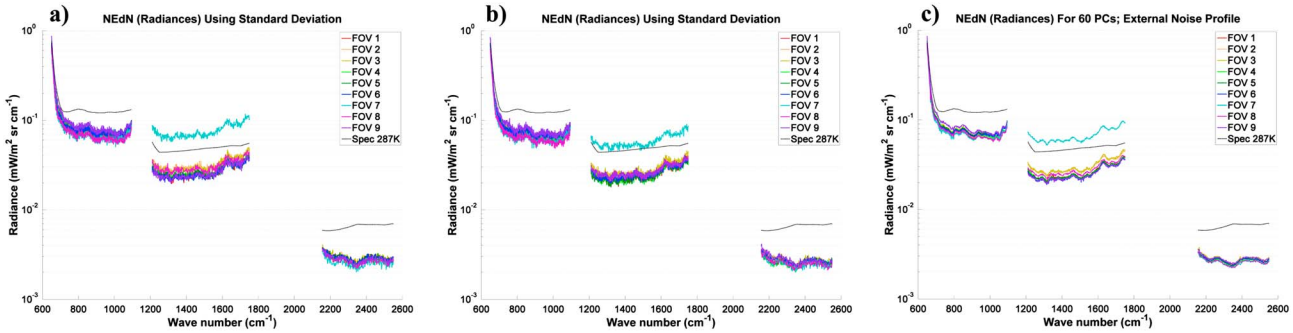

Figure 5. NEdN estimated from (a) ICT, (b) DS, and (c) ES data acquired on 10 January 2013, Orbit 6245.

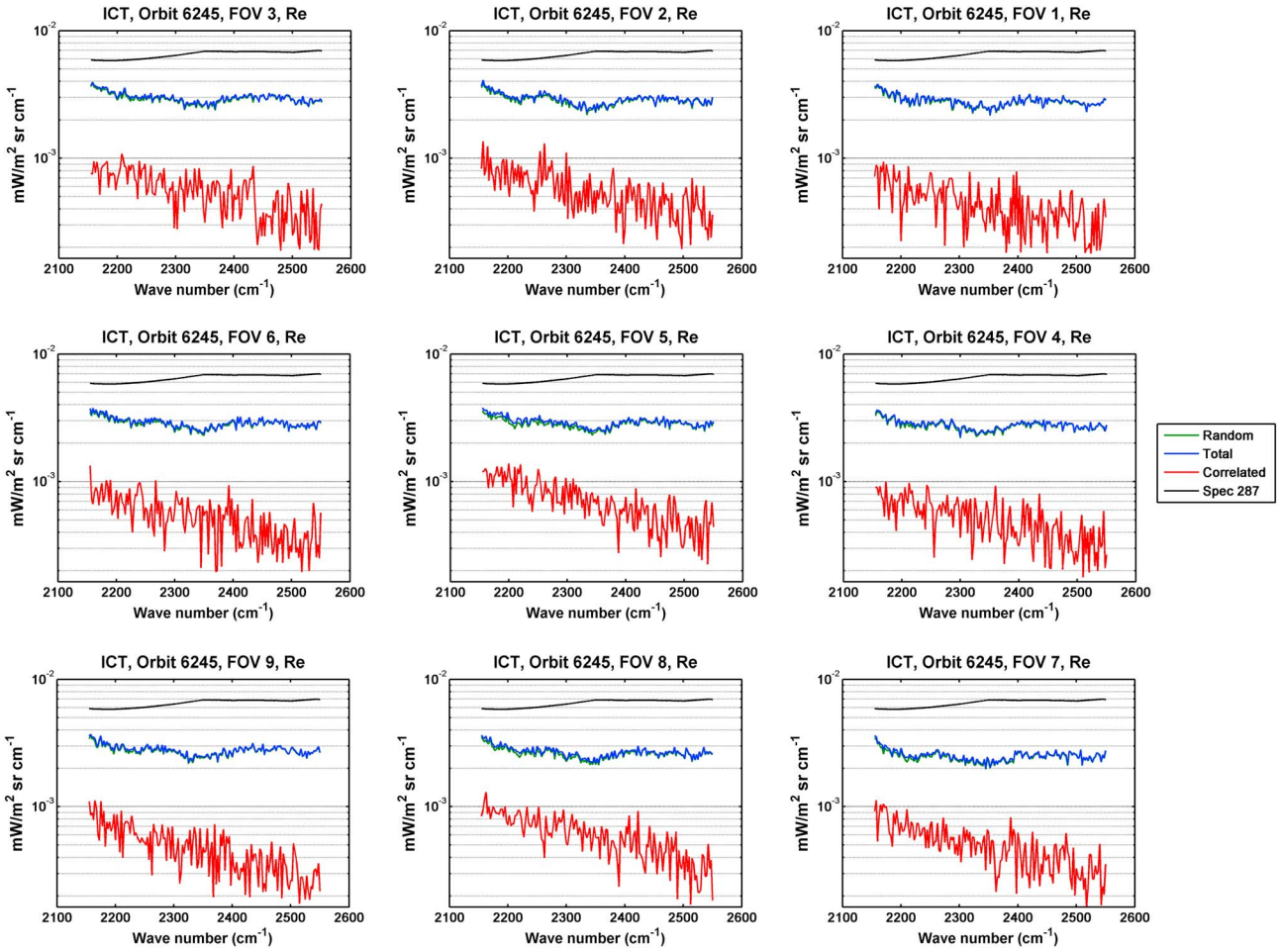

Figure 6. Random/correlated noise contribution to the total NEdN in SWIR spectral band estimated for all nine FOVs from the ICT data acquired on 10 January 2013, Orbit 6245. Note that the blue line (total noise) overlays the green line (random noise).

4.1. Real Spectra NEdN

[44] Figure 5 shows the total NEdN estimated from ICT (Figure 5a) and DS (Figure 5b) calibrated spectra along with the random NEdN component estimated from the ES data (Figure 5c). On-orbit instrument NEdN is practically the same as during TVAC4 and the spacecraft TVAC ground tests. NEdNs estimated from all three targets agree very well. Small differences between ICT, DS, and ES NEdNs are due to different target temperatures. The NEdN estimated from the DS view is the lowest because at the deep space temperature of ~4 K the instrument sees the lowest radiance fluxes emitted by the instrument itself. The NEdN of MWIR FOV7 is slightly out of spec as was previously discovered during TVAC4 and spacecraft TVAC ground tests. The NEdN of all other FOVs are well within mission requirements in all three spectral bands.

[45] PCA analysis has shown that practically no contribution of spectrally correlated noise is observed in either ICT- or DS-derived NEdN in all spectral bands. An example of negligible contribution of spectrally correlated noise to the total NEdN estimated for all nine FOVs using SWIR ICT spectra (most sensitive to the external vibration) is shown in Figure 6. The same pattern is observed in the LWIR and MWIR spectral bands for both ICT and DS views.

[46] The noise performance of the CrIS instrument has remained stable throughout the on-orbit sensor operation, and no anomalies have been observed. Figure 7 shows the NEdN trend from 21 January 2012 to 31 August 2013 based on the ICT derived NEdN. The results from 160 scan lines (40 granules) near the same tropical region were processed every 3–6 days. The NEdN was averaged over all FOVs and over the following spectral regions: LWIR band (650–750, 750–900, and 750–1950 cm^{-1}), MWIR entire band (1210–1750 cm^{-1}), and SWIR entire band (2155–2550 cm^{-1}). The LWIR spectral region 650–700 cm^{-1} was chosen to monitor beamsplitter transmittance trend, while the LWIR 750–900 cm^{-1} spectral region was chosen as an indicator of possible ice contamination. The DS-derived NEdN trend shows the same consistency and stability as the ICT NEdN.

[47] Only small seasonal, orbital, and spatial variations in the NEdN are observed in orbit. The CrIS NEdN is dominated by the instrument background radiation (see Figure 1), which is very stable. By design, the CrIS optical bench is thermally buffered from the rest of the CrIS structure which results in an optical bench temperature change of typically ±50 mK over an entire orbit. This keeps the temperature of the interferometer optics, telescope, and aft band separation optics which produce the dominant CrIS instrument

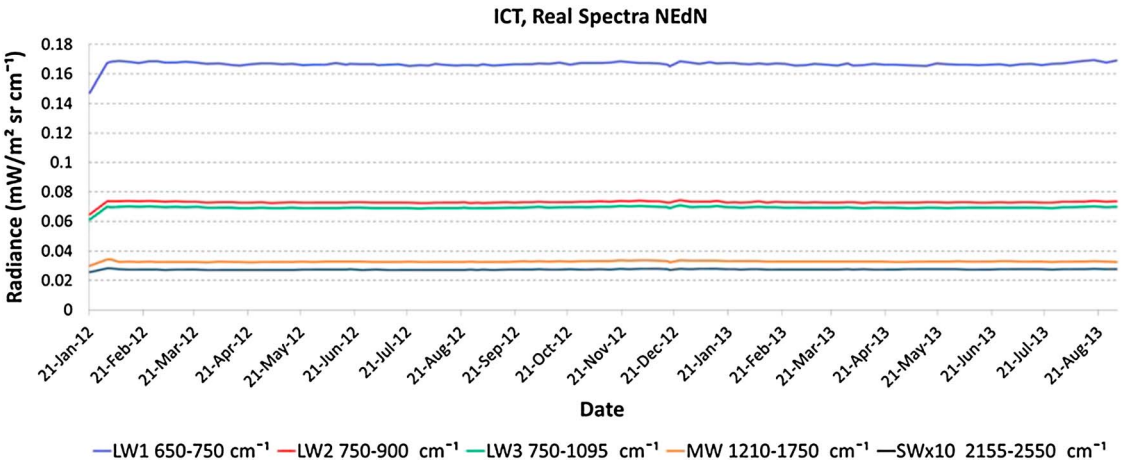

Figure 7. Trend of the average NEdN in selected spectral regions over 21 January 2012 to 31 August 2013 derived from the ICT NEdN acquired over the same tropical region 30°S–30°N and 160°E–150°W.

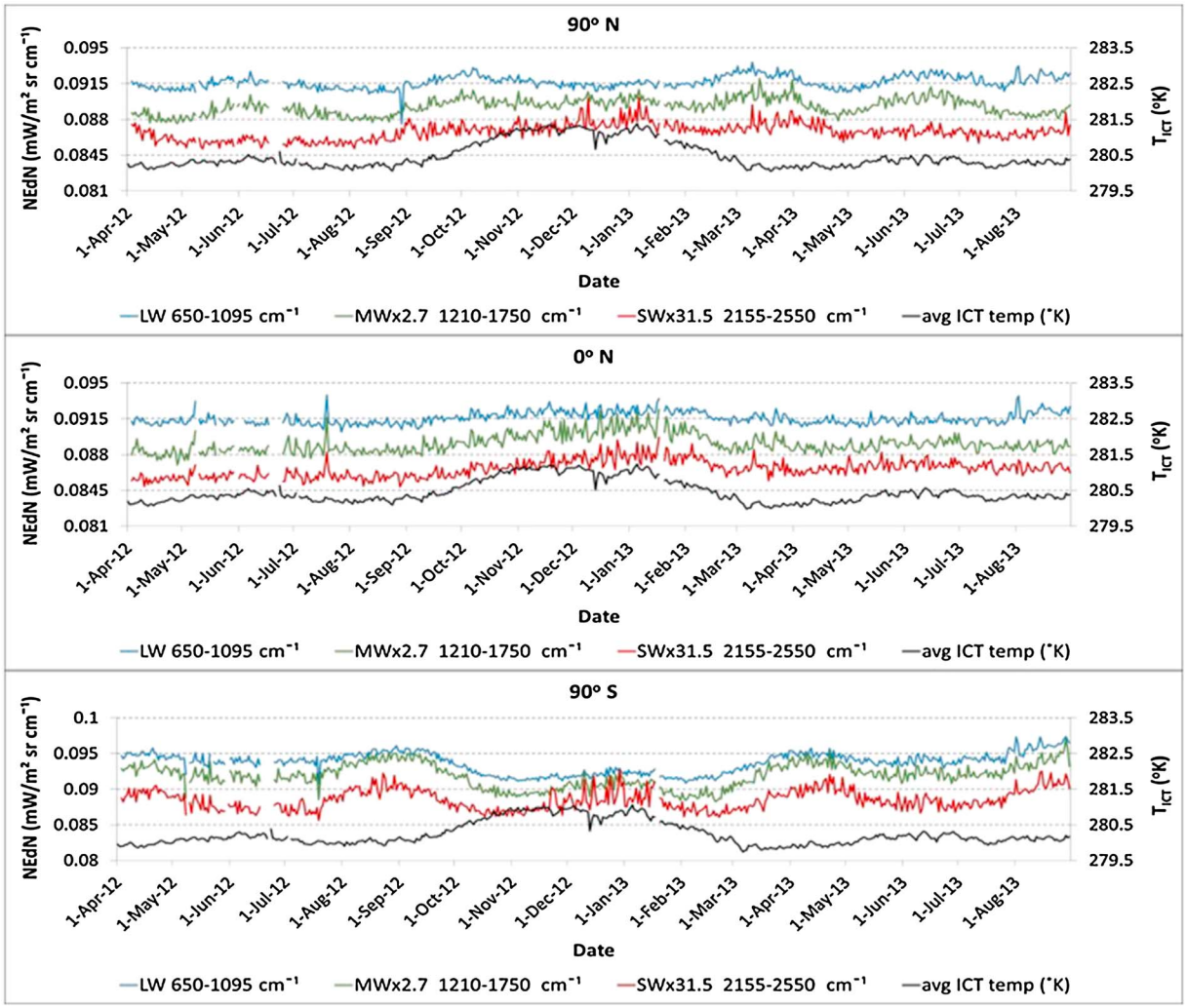

Figure 8. Seasonal variation of average NEdN observed over the North Pole (90°N), equator (0°N), and South Pole (90°S) regions. The NEdN is scaled up by a factor of ×2.7 in MWIR and by ×31.5 in LWIR spectral bands. The ICT temperature trend at the same location is shown by the black line.

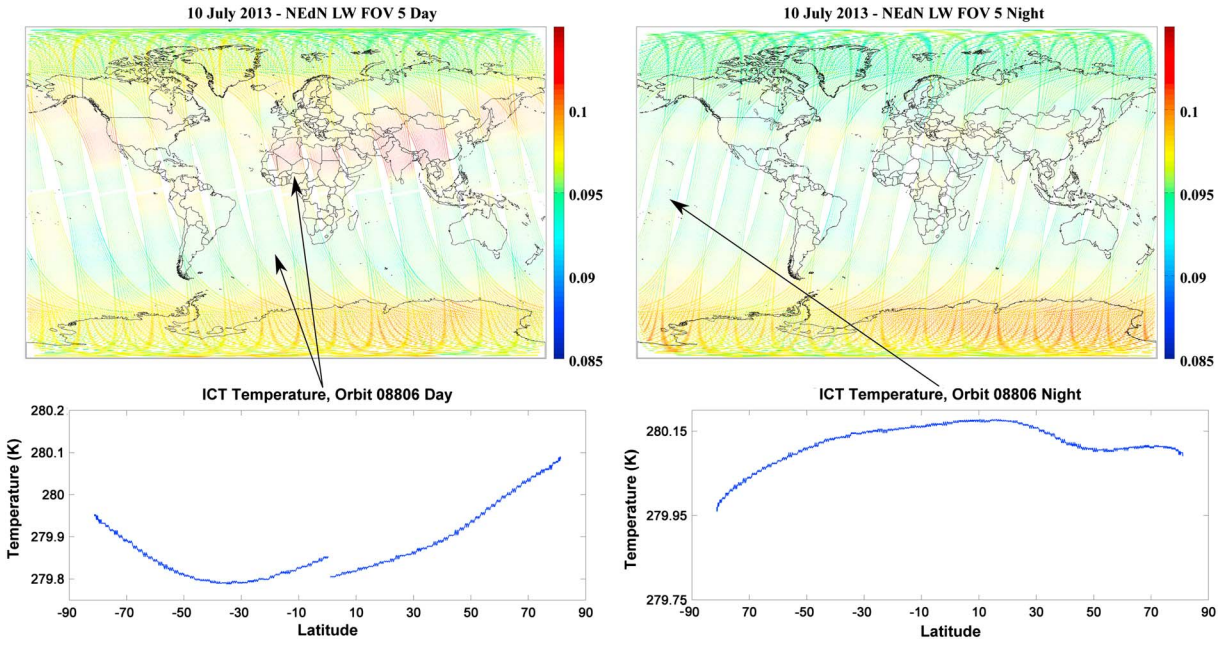

Figure 9. Orbital and spatial distribution of the LWIR FOV5 NEdN observed on 10 July 2013 for ascending (day) and descending orbits (night). NEdN is averaged over the whole spectral band and plotted in standard radiance units ($mW/m^2\,sr\,cm^{-1}$) with a margin of ±10% from the nominal NEdN value. Bottom graphs show the ICT temperature variation for a single orbit #08806 marked by the arrows (latitude 90 represents the North Pole, while −90 represents the South Pole).

background invariant over an entire orbit. In addition, band-limiting filters are passively cooled and thermally stabilized. It is also important to note that the CrIS instrument background radiation is approximately 4 times larger than the photon flux from the warmest Earth scene viewed by CrIS in all of its three infrared bands. Thus, it is expected that CrIS NEdN will not change significantly for any type of Earth scene viewed, for ICT views, or for the small thermal variations of optical bench that occur over an orbit.

[48] In Figure 8 the seasonal trend in the NEdN is plotted at a small scale to capture NEdN variations of the order of few percent of the average. The NEdN data were acquired from the official CrIS SDR product at nadir at different orbital positions once a day and averaged over each spectral band and over nine FOVs. To compare noise variations in all three spectral bands, the MWIR and SWIR NEdN have been scaled up to match the LWIR NEdN value. The ICT temperature is acquired at the same locations and plotted on the graphs.

[49] At low latitude (~ 65°North to −65°South) the NEdN seasonal variations do not exceed 2–3% and in general correlate with the seasonal variations of the ICT temperature following the variation in thermal environment (CrIS ICT target is not temperature controlled and floats with the instrument temperature). Slightly larger variations ~ 4–6% are observed over the South Pole. NEdN over both North and South Pole regions exhibit additional seasonal variations during spring and fall. In Figure 9 the orbital and spatial variations in LWIR FOV5 NEdN are shown for ascending (daytime) and descending (nighttime) orbits on 10 July 2013. FOV5 was chosen to illustrate the very small variations in the NEdN <10% and is typical of the small noise variations in each FOV. The same general NEdN variation pattern is observed in the MWIR and SWIR FOVs/detectors. The ICT temperature variation is shown in the bottom graphs for orbit # 08806 for both the ascending and descending parts of the orbit. The apparent discontinuity in the ICT temperature in Figure 9 (left) is caused from the first part of the graph being from the end of the orbit and the last part being from the start.

[50] It is clearly seen that NEdN variations over the North and South Poles do not follow the instrument temperature (as occurs in the tropics) exhibiting slightly larger noise over the South Pole region where the ICT temperature is the lowest. The spacecraft transition over the North Pole always occurs from the day part of the orbit to the night part, while the transition over the South Pole is night to day. During night/day transition over the South Pole the sunlight hits the spacecraft about 8 min earlier than night/day transition on the Earth due to the NPP orbit altitude of 828 km. The light/thermal shock induced by the sunlight interaction during this transition could be the cause of this slight noise increase. There are also some small spatial NEdN variations during daytime (see Figure 9 over the Africa and Asia). The effect of sunlight interaction with the CrIS instrument and small spatial NEdN variations during daytime are not clearly understood and are under investigation.

[51] Nevertheless, temporal, orbital, and spatial variations in the NEdN are very small in all spectral bands, and FOVs and do not exceed 10% of the NEdN nominal values. No NEdN anomalies are observed over the South Atlantic Anomaly region as illustrated in Figure 9 for both ascending and descending orbits. This is true for all spectral bands and all FOVs/detectors. Note that for almost 2 years of on-orbit operations, there have been very few events where the CrIS instrument impulse noise exceeds its threshold. The relatively large area of PV HgCdTe detectors (1 mm in diameter)

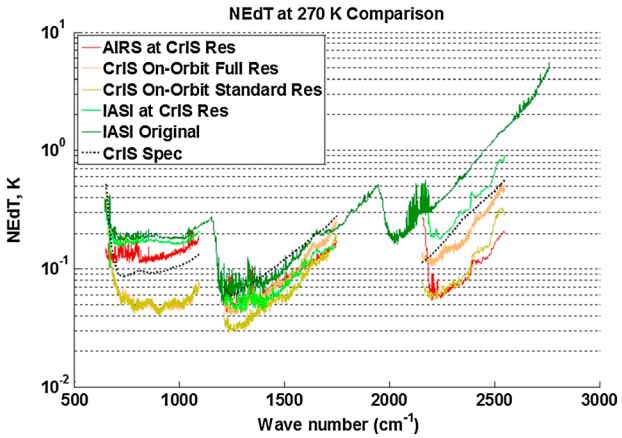

Figure 10. CrIS on-orbit nominal NEdT is compared with AIRS (at CrIS spectral resolution) and IASI NEdT estimated at IASI original and CrIS-like spectral resolution. The black curve depicts CrIS spec requirements. NEdT was estimated for scene temperature of 270 K.

and radiation shielding provide reliable protection of the detector array from the high-energy particle irradiation [*Kelly et al*., 2003]. In addition, digital signal processing onboard CrIS uses triple mode redundancy in processing of all interferograms which makes the electronics robust to single-event upsets due to the space radiation environment.

[52] Overall, the in-flight CrIS noise performance can be summarized as follows:

[53] 1. NEdN level meets mission requirements in all spectral channels with a large margin of typically 100% (except MWIR FOV 7) and is consistent with ground tests.

[54] 2. The intrinsic detector noise randomly distributed in spectral domain dominates total instrument NEdN. Negligible contribution of correlated noise is observed.

[55] 3. No degradation of CrIS NEdN has been observed since spacecraft TVAC ground testing and the NEdN has remained extremely stable during on-orbit operations.

[56] 4. CrIS NEdN exhibits slight seasonal, orbital, and spatial variations (on the level of 2–4% of the nominal value) consistent with the change in the thermal instrument environment for most of the orbit. Slightly larger variations (4–6%) are observed over the North and South Pole regions during night-day transitions. All seasonal, orbital, and spatial variations are small, do not exceed 10%, and have negligible impact on the quality of the CrIS SDR product.

[57] 5. CrIS has comparable or smaller noise levels than AIRS and IASI heritage instruments as demonstrated in Figure 10. Noise equivalent differential temperature (NEdT) is shown for all three sensors at scene temperature of 270 K. NEdT was estimated from the operational Earth scene data using PCA technique. CrIS NEdT was estimated for standard and full spectral resolution of 0.625 cm^{-1} in all spectral bands using data acquired during on-orbit full-resolution test.

[58] 6. As expected, CrIS full spectral resolution noise in MWIR and SWIR bands is higher by ~×1.4 and ~×2, respectively, as compared to the CrIS standard spectral resolution (see Figure 10).

4.2. Imaginary Spectra Noise

[59] The excellent noise performance of CrIS SDR in the real part of the spectra reflects the quality of the calibrated real radiances that are typically used in the EDR algorithms and assimilated to the NWP weather and climate prediction models. The imaginary part of the SDR spectra which is normally discarded and not used to develop atmospheric profile products has a unique diagnostic role for instrument operation. The imaginary SDR spectra noise can be used to detect the presence of correlated noise and do so with a much higher sensitivity than is possible using the real SDR spectra. Thus, any signal distortions of the interferogram in the OPD domain due to sampling, delay, tilt alignment, jitter, etc. can be detected well before they become apparent in the real SDR products. Analysis of the CrIS on-orbit data and reanalysis of the TVAC data have shown that NEdN estimated from the imaginary part of the calibrated spectra is most sensitive to any external disturbances and artifacts, including vibration. In this section preliminary results of noise analysis for the imaginary spectra are presented and compared with ground test data.

[60] Figure 11 shows the total NEdNs of the imaginary spectra estimated as the standard deviation of each spectral channel for ICT measurements (Figure 11a), DS measurements (Figure 11b), and ES measurements (Figure 11c). Typically, ES imaginary spectra have weak atmospherically induced spectral correlation so that total ES noise induced

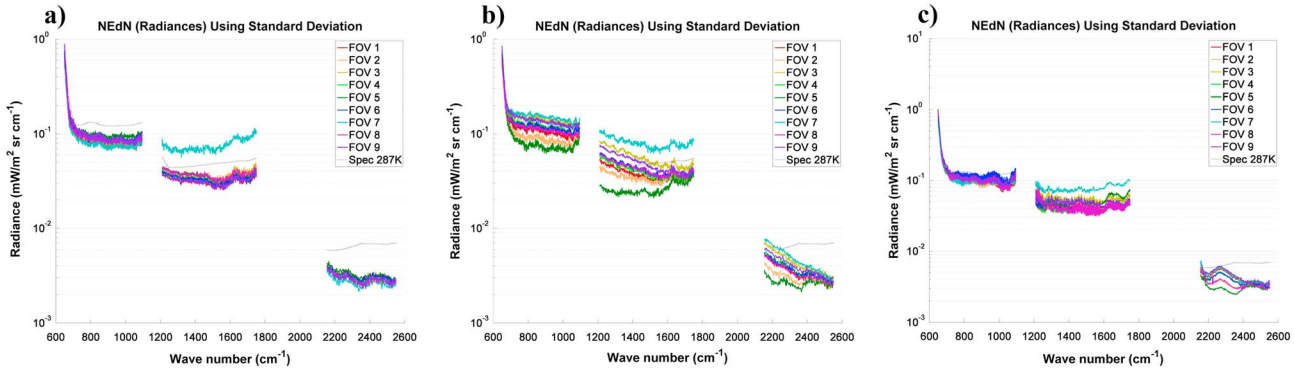

Figure 11. Total NEdN estimated from the imaginary part of (a) ICT, (b) DS, and (c) ES spectra acquired on 10 January 2013, Orbit 6245.

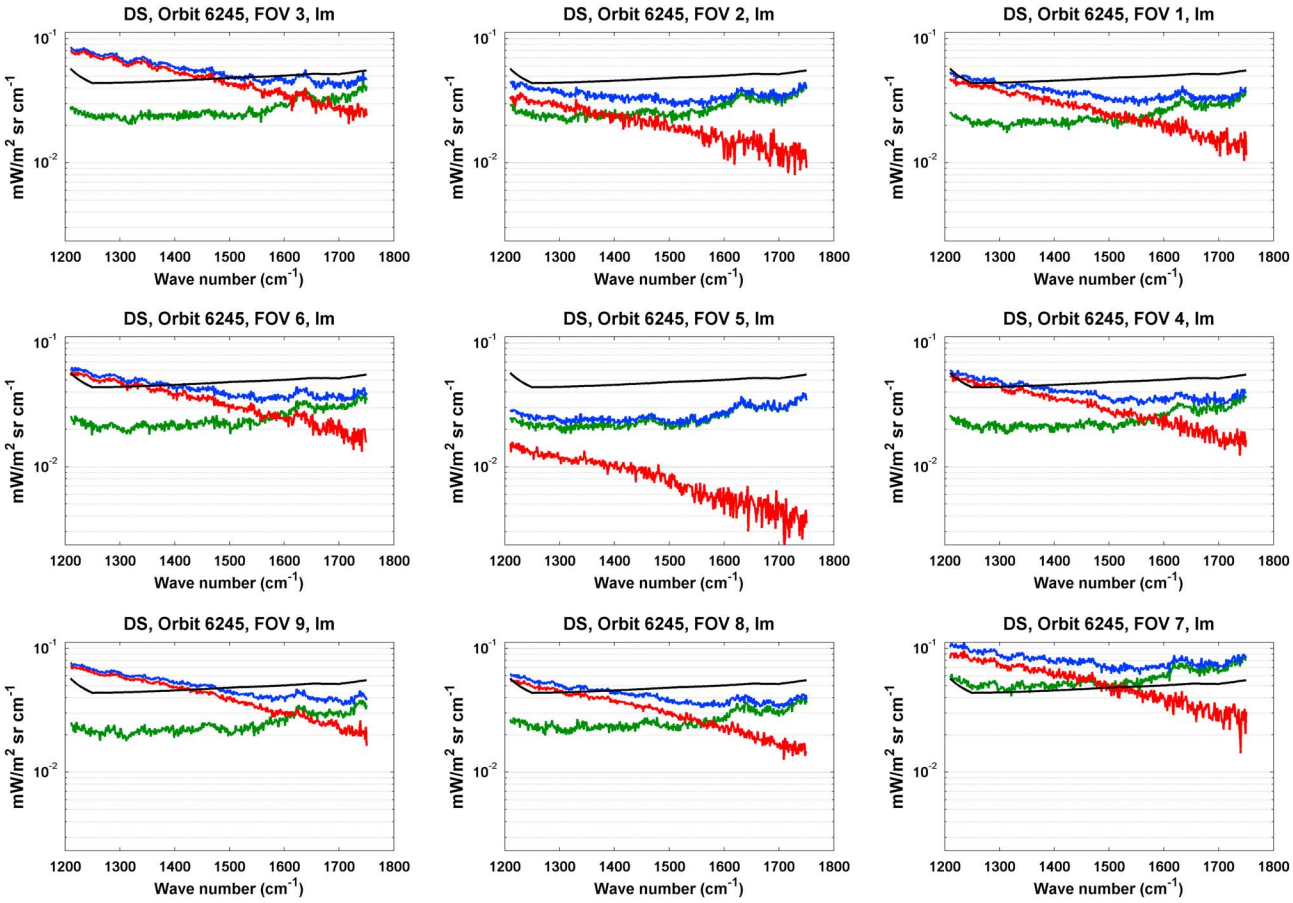

Figure 12. Random/correlated noise contribution to the total imaginary NEdN in MWIR spectral band estimated for all nine FOVs from DS data acquired on 10 January 2013, Orbit 6245.

by the instrument itself can be estimated as the standard deviation, as in the case of ICT and DS targets. The random NEdN component estimated from the same data set using the PCA technique is practically on the same level as the real NEdN spectra shown in Figure 5. This means that the lowest possible noise in the imaginary spectra is determined by the intrinsic detector noise, while higher noise levels in the imaginary spectra are totally due to the correlated noise component.

[61] The validity of this conclusion is demonstrated in Figure 12 where random/correlated noise contributions to the total NEdN estimated from DS MWIR imaginary spectra are shown for all nine FOVs/detectors. Similar patterns are observed in MWIR and SWIR spectral bands.

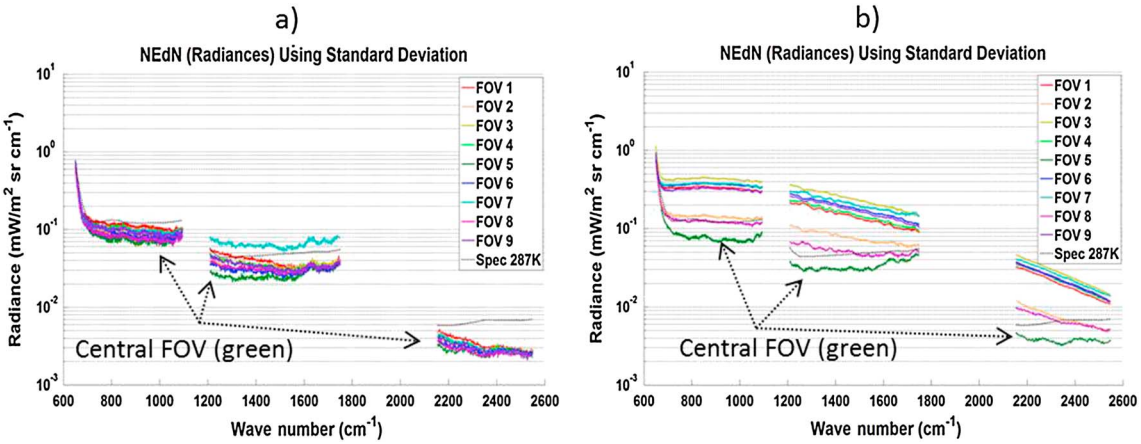

Figure 13. (a) Total NEdN estimated from the imaginary part of DS spectra acquired during orbit 5266 on 11 November 2012 and (b) total NEdN estimated from the imaginary DS spectra acquired during TVAC4 PQH test.

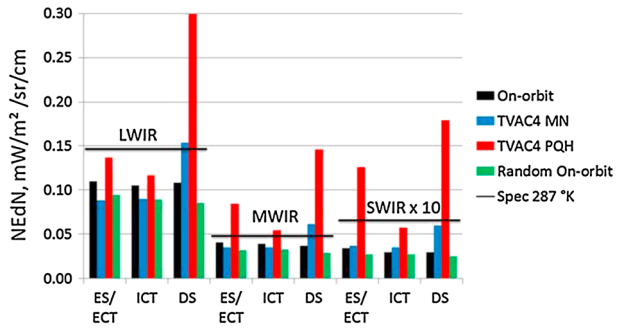

Figure 14. Total imaginary NEdN observed on orbit and during TVAC4 MN and PQH tests. NEdN was averaged over each spectral band and all FOVs. Random noise level estimated from the on-orbit imaginary spectra is shown in green. Average specification noise level is also shown (black lines).

[62] Figure 12 clearly shows that center FOV 5 exhibits a very small contribution of the correlated noise, while the largest correlated noise occurs in the corner FOVs (1, 3, 7, and 9). This is a typical signature of the interferometer tilt-induced OPD sample jitter noise when off-axis corner FOVs experience larger jitter of the mirror alignment (tilt jitter). Reanalysis of the TVAC data has shown that during all test steps the imaginary part of the spectra exhibited significantly higher noise than the same noise determined from the real part of the spectra for all three targets, with the DS target exhibiting a significantly higher imaginary noise level. In Figure 13, the total imaginary noise estimated from the DS target on orbit (Figure 13a) is compared with total imaginary DS noise estimated during TVAC4 PQH test (Figure 13b). It is seen that the level of total imaginary noise during TVAC testing was significantly higher than that measured in orbit. PCA analysis has shown that all elevated noise during the TVAC tests was also due to the correlated noise component originating from test facility vibration. The larger noise in the imaginary spectra was observed for corner FOVs, while the center FOV5 exhibited the lowest noise, which was on the level of the random detector noise (Figure 13b).

[63] In Figure 14 the average level of imaginary noise observed on orbit for all three targets is compared with imaginary NEdN observed during TVAC4. The NEdNs plotted on this graph were averaged over each spectral band and over nine FOVs/detectors. It should be noted that during TVAC tests a residual vibration from the test equipment was present, and this vibration significantly exceeded in-flight vibration levels especially during the PQH TVAC4 test. This residual vibration only slightly affected the real spectra NEdN (section 3.3), while its effect on the imaginary noise was more pronounced.

[64] The results of the NEdN estimated from the imaginary part of the calibrated complex spectra reported in this section are preliminary, and detailed analysis is continuing. The following observations can be made about the preliminary data:

[65] 1. NEdN estimated from the imaginary spectra exhibits elevated level for all three targets (ICT, DS, and ES) due to the spectrally correlated noise component. Random noise is on the same level as real spectra NEdN and is dominated by the intrinsic detector noise.

[66] 2. On-orbit imaginary NEdN is significantly smaller than NEdN observed during ground tests when a residual vibration from the test equipment was present.

[67] 3. Imaginary NEdN is extremely sensitive to any instrument artifacts and external vibration as compared to the real NEdN. Corner FOVs are more susceptible to the tilt-induced OPD sample jitter. DS-derived imaginary NEdN has largest vibration sensitivity, while ICT target exhibits the smallest vibration susceptibility.

[68] 4. Elevated imaginary noise reflects small instabilities of the phase of the complex calibrated spectra and has no impact on the calibrated real SDR spectra and its NEdN.

5. Summary

[69] The CrIS on-orbit NEdN performance is outstanding and meets all requirements for the NPP/JPSS mission. The instrument on-orbit noise has been stable and consistent with the last spacecraft ground test sequence and on-orbit operations from instrument activation on 21 January 2012. The overall noise level is better than spec requirements in all spectral bands and all FOVs (except MWIR FOV 7) and is comparable or better than NEdN performance of AIRS and IASI heritage instruments. The results of noise modeling and analysis of ground and on-orbit data have shown that the total CrIS NEdN is limited by the intrinsic detector noise randomly distributed in the spectral domain.

[70] The CrIS interferometer and its dynamic optical alignment system design along with accurate sampling, filtering, and calibration procedures implemented in the operational SDR algorithm reduced alignment jitter and sampling artifacts to a minimum so that the contribution of the correlated noise component to the total CrIS NEdN is negligible. The resulting CrIS noise covariance matrix is purely diagonal, which is specifically important for the CrIS SDR product users dealing with atmospheric profile retrievals and SDR data assimilation in meteorological and climatology prediction models. It should be noted that excellent noise performance of the instrument has been achieved even without engaging vibration-isolation system designed to damp any possible vibration coming from other instruments and spacecraft platform of the Suomi NPP mission.

[71] On-orbit and ground test data analysis showed that noise determined from the imaginary part of the complex calibrated radiance spectra exhibits higher sensitivity to various FTS instrument artifacts including vibration. To the best of our knowledge, this is a first attempt to analyze noise estimated from the imaginary radiance spectra. The imaginary part of the spectra is useful for assessing the phase stability of the FTS instrument and any additional errors in the interferogram domain due to OPD sampling, delays, optical alignment (tilt), jitter, etc. that may cause additional noise in the imaginary part of the FTS spectra. Therefore, the imaginary NEdN can be used to assess and monitor FTS instrument health while on orbit. All three on-orbit views (ES, ICT, and DS) exhibit slightly elevated imaginary NEdN on top of the random noise determined by the intrinsic detector noise. This elevated noise is correlated in the spectral domain, and as a rule, the corner FOVs exhibit a higher noise level, which is characteristic for the vibration-induced optical tilt jitter. Imaginary DS-derived NEdN appears to be most sensitive to these instabilities as compared to the ES and ICT targets. On-orbit imaginary NEdN is significantly smaller than that observed during ground testing where residual vibration from the test equipment was present. However,

this slightly elevated imaginary noise level has no impact on the real spectra-derived NEdN. The CrIS real calibrated radiances have small, stable, and spectrally uncorrelated noise level.

[72] **Acknowledgments.** The authors wish to acknowledge that this work was funded and supported by NOAA STAR and the JPSS program. The support of the JPSS program is recognized and appreciated. Although every effort has been made to insure that the content of this article is accurate, any mistakes are the responsibility of the authors.

References

Antonelli, P., H. E. Revercomb, and L. A. Sromovsky (2004), A principal component noise filter for high spectral resolution infrared measurements, *J. Geophys. Res.*, *109*, D23102, doi:10.1029/2004JD004862.

Aumann, H. H., et al. (2003), AIRS/AMSU/HSB on the Aqua Mission: Design, science objectives, data products, and processing systems, *IEEE Trans. Geosci. Remote Sens.*, *41*, 410–417.

Barnet, C. D., J. M. Blaisdell, and J. Susskind (2000), Practical methods for rapid and accurate computation of interferometric spectra for remote sensing applications, *IEEE Trans. Geosci. Remote Sens.*, *38*, 169–183.

Glumb, R. J., and D. C. Jordan (2000), Enhancements to the Crosstrack infrared sounder (CrIS) for improved radiometric accuracy, *Proc. SPIE*, *4131*, 323–333, doi:10.1117/12.406555.

Glumb, R. J., D. C. Jordan, and P. Mantica (2002), Development of the Crosstrack Infrared Sounder (CrIS) sensor design, *Proc. SPIE*, *4486*, 411–424, doi:10.1117/12.455124.

Han, Y., et al. (2013), Suomi NPP CrIS measurements, sensor data record algorithm, calibration and validation activities, and record data quality, *J. Geophys. Res. Atmos.*, *118*, 12,734–12,748, doi:10.1002/2013JD020344.

Kelly, M. W., E. J. Ringdahl, A. I. D'Souza, S. D. Luce, and E. W. Cascio (2003), Proton irradiations of large area Hg1-xCdxTe photovoltaic detectors for the Cross-track Infrared Sounder, *Proc. SPIE Infrared Technol. Appl.*, *4820*, 479–490.

Klaes, K. D., et al. (2007), An introduction to the EUMETSAT polar system, *Bull. Am. Meteorol. Soc.*, *88*, 1085–1096.

Masterjohn, S. A., A. I. D'Souza, L. C. Dawson, P. N. Dolan, P. S. Wijewarnasuriya, and J. C. Ehlert (2003), Cross-track infrared sounder FPAA performance, Proc. SPIE. 4820, Infrared Technology and Applications XXVIII 368 (January 1) doi:10.1117/12.453568.

Schwantes, K., D. Cohen, P. Mantica, and R. J. Glumb (2002), Modeling Noise Equivalent Change in Radiance (NEdN) for the Cross-track Infrared Sounder (CrIS), *Proc. SPIE*, *4486*, 456, doi:10.1117/12.455128.

Smith, W. L., H. Revercomb, G. Bingham, A. Larar, H. Huang, D. Zhou, J. Li, X. Liu, and S. Kireev (2009), Technical note: Evolution, current capabilities, and future advances in satellite ultra-spectral IR sounding of the lower atmosphere, *Atmos. Chem. Phys.*, *9*, 5563–5574.

Smith, W. L., E. Weisz, S. Kireev, D. Zhou, Z. Li, and E. E. Borbas (2012), Dual-Regression Retrieval Algorithm for real-time processing of satellite ultra-spectral radiances, *J. Appl. Meteorol. Clim.*, *51*, 1455–1476, doi:10.1175/JAMC-D-11-0173.1.

Tobin, D., H. Revercomb, P. Antonelli, K. Vinson, S. Dutcher, R. Knuteson, J. Taylor, F. Best, C. Moeller, and M. Gunshor (2006), Recent efforts to validate EOS observations. Hyperspectral data noise characterization using PCA: Application to AIRS, in *Proc. SPIE Optics and Photonics*, vol. 6301, pp. 630,107.

Tobin, D., et al. (2013), Suomi-NPP CrIS radiometric calibration uncertainty, *J. Geophys. Res. Atmos.*, *118*, 10,589–10,600, doi:10.1002/jgrd.50809.

Zachor, A. (1977), Drive non-linearities: Their effects in Fourier spectroscopy, *Appl. Opt.*, *16*, 1412–1422.

Zavyalov, V. V., C. S. Fish, G. E. Bingham, M. Esplin, M. Greenman, D. Scott, and Y. Han (2011), Preflight assessment of the cross-track infrared sounder (CrIS) performance, *Proc. SPIE Eur. Atmos. Remote Sens.*, *8176*, 817,606.